Surface Chemical Control of Mechanical Energy Losses in Micromachined Silicon Structures

Yu Wang,[†] Joshua A. Henry,[†] Alan T. Zehnder,[‡] and Melissa A. Hines*[,†]

Departments of Chemistry and Theoretical and Applied Mechanics, Cornell University, Ithaca, New York 14853

Received: July 12, 2003; In Final Form: October 29, 2003

Mechanical energy dissipation in room-temperature micromechanical silicon torsional resonators, with resonant frequencies ranging from 2.2 to 23 MHz, is considerably increased when a single monolayer of hydrogen atoms is replaced by 13 Å of silicon oxide (which corresponds to the oxidation of less than 2 silicon bilayers.) Measurements of oxidation-induced resonant frequency shifts show that increased dissipation cannot be attributed to chemically induced changes in the stress or tension of the resonator. The dependence of both the frequency shift and reduction in quality factor on resonator size are consistent with a chemically induced surface loss mechanism. Quantitative analysis shows that even relatively unstressed areas of the surface can contribute considerably to mechanical energy dissipation. The scaling of losses with resonator dimensions suggests that surface effects will become increasingly more important as the sizes of micromechanical devices continue to decrease.

I. Introduction

As technological advances allow smaller and smaller devices to be fabricated, at what point will surface chemistry begin to affect the mechanical properties of the devices? In the following, we show that surface chemistry has an effect on the dynamic properties of surprisingly large devices—devices that are easily fabricated with standard lithographic techniques. More importantly, a quantitative analysis of these effects suggests that careful attention to surface chemistry will be necessary for the fabrication of high-performance nanomechanical resonators.

Mechanical resonators play an important role in many technologies, and the development of high-performance micromechanical resonators would enable advances in many applications, including mass spectrometry,[1] calorimetry,[2] scanned probe microscopy,[3] electrometry,[4] and perhaps even cellular telephony.[5] For example, the minimum detectable force in a scanned probe microscope is inversely proportional to the fQ product of the sensing cantilever, where f and Q are the cantilever's frequency and quality factor, respectively.[6] (The Q of a resonator is proportional to the number of free oscillations the resonator will undergo after an initial excitation and is inversely proportional to the rate of mechanical energy dissipation.)

Advances in nanofabrication have enabled the production of very high-frequency resonators (e.g., 380 MHz[7]); however, these increases have been accompanied by puzzling decreases in quality. A general trend toward decreasing quality with decreasing resonator size has led to the suggestion that surface effects may influence resonator behavior.[8,9]

In the following, we show that surface chemistry can play an important role in determining the quality of micromechanical silicon resonators, even at room temperature. By chemically modifying *only the surface* of the resonator, the resonator's Q can be increased considerably. By quantitatively studying the scaling behavior, we show that this effect is both chemical and atomic scale; it is not due to size- or chemical-induced changes in static mechanical properties, nor is it due to changes in the static stress or tension of the resonator. Our analysis shows that this effect will become increasingly more important as the size of the resonator shrinks. This effect also shows unexpected scaling behavior with resonator size, as even relatively unstressed regions of surface contribute to mechanical losses.

In macroscopic systems, chemically induced mechanical energy dissipation is only important at extremely low temperatures. For example, boron dopants considerably increase dissipation in macroscopic silicon oscillators near 7 mK.[11] This dissipation is due to periodic, stress-induced shifts in the electronic energy levels of boron-induced holes. In room-temperature macroscopic silicon resonators, these small chemical losses are overwhelmed by intrinsic thermoelastic losses. Pure silicon dioxide (i.e., amorphous silica) resonators have exceedingly low mechanical losses, even at room temperature.[12] Since crystalline silicon and silica are low-loss materials that are expected to have the same intrinsic losses at room temperature,[13] mechanical energy dissipation by the thin native oxide (∼10 Å) that covers most silicon devices has often been overlooked.

Studies of surface chemistry-induced mechanical energy dissipation are very challenging, as there are many pathways for dissipation in micromechanical devices. For example, direct coupling to the supporting structure leads to so-called clamping losses which, in many cases, dominate other losses. To isolate the effects of surfaces, we studied the scaling behavior of the mechanical losses in a series of suspended micromechanical oscillators, such as the one shown in Figure 1. All of the oscillators were suspended by 4 μm long, 440 nm wide silicon "wires." The width of the paddles (measured across the flats) was systematically varied from ∼2.5 to 7 μm to change the mass and moment of inertia of the load, whereas the thickness of both the paddle and wires was varied from ∼190 to 240 nm by chemical etching. As illustrated in Figure 2, this design conserves a large area of the resonators, including the highly

* Corresponding author. E-mail: Melissa.Hines@cornell.edu.
[†] Department of Chemistry.
[‡] Department of Theoretical and Applied Mechanics.

10.1021/jp0360164 CCC: $25.00
Published on Web 12/03/2003

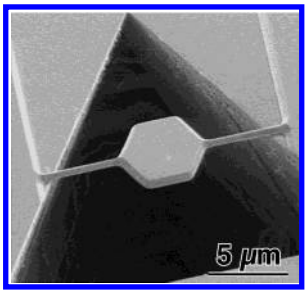

Figure 1. Scanning electron micrograph of suspended silicon paddle resonator.

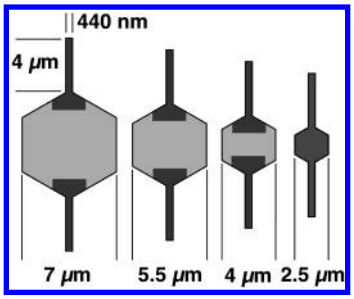

Figure 2. Four different paddle geometries. The shaded regions represent areas that are conserved across the series.

stressed wire and wire/paddle junction, while varying the relatively unstressed paddle surface.

The {111} surfaces of silicon were chosen for their chemical properties, as aqueous etching techniques can be used to produce extremely homogeneous, H-terminated Si(111) surfaces[14] with ultralow defect densities[15] and very low surface stress.[16] In the following experiments, {111} faces of silicon make up 70−85% of the surface area of each paddle. The hexagonal shape of the oscillators and triangular shape of the enclosing pits take advantage of the 3-fold symmetry of this surface. This design minimizes the number of different silicon faces (and thus different surface chemistries) on each paddle and prevents undercutting of the wire supports.

II. Experimental Section

Suspended micromechanical oscillators were fabricated from single crystal Si(111) wafers using a combination of optical lithography, reactive ion etching, and wet chemistry. The primary objective in this study was the production and characterization of defect-free micromechanical devices with well-controlled and well-characterized Si{111} surfaces. As such, the resonators were fabricated from single crystal wafers, not silicon-on-insulator substrates. Critical point drying, which is known to cause gross surface contamination, was not used. Metalization of the resonators and substrates, which can cause both surface contamination and increased mechanical energy dissipation, was specifically avoided.

The fabrication process is similar to that used by Ensell.[17] Figure 3 illustrates the process in cross-section. The lateral shape of the paddles, wires, and enclosing triangular wells were first defined using optical lithography. The paddles and wires were then formed by reactive ion etching (RIE), as shown in Figure 3b. The defined structure was protected with a 100 nm thick, well annealed thermal oxide layer (Figure 3c); then 10 μm deep trenches were defined around the protected resonator structure using a second stage of optical lithography and RIE (Figure 3d). The triangular shape and orientation of the trenches were chosen to minimize undercutting during subsequent processing. To release the paddles from the bulk silicon, the sample chip

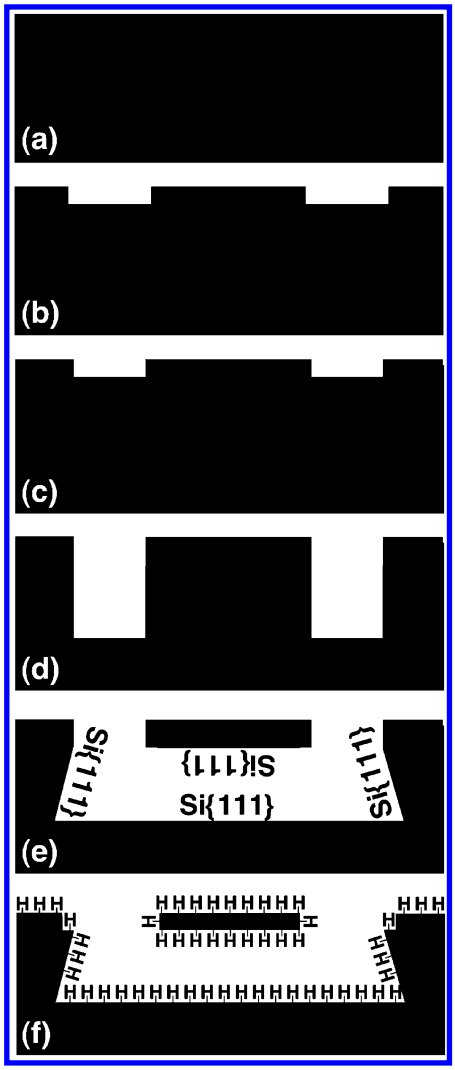

Figure 3. Microfabrication process in cross-section (not to scale). Si is shown in black, whereas SiO_2 is gray. Key: (a) initial Si(111) wafer; (b) dhape of paddles, wires, and enclosing trenches defined using optical lithography and RIE; (c) protective SiO_2 layer applied; (d) feep trenches defined using lithography and RIE; (e) KOH etch removed all non-Si{111} faces; (f) oxide stripped with NH_4F/HF leaving a H-terminated surface.

was first scrupulously cleaned using a modified RCA clean, as described in ref 18. The cleaned chip was then etched in 50% w/v KOH(aq) at 70 °C for 5−8 min and rinsed in ultrapure water (Millipore Milli-Q). Aqueous KOH is a highly anisotropic silicon etchant that selectively removes all non-{111} silicon planes[19] without etching the protective SiO_2 layer, as shown in Figure 3e. After release, KOH continued to etch the backside of the paddle, albeit very slowly. Because of this, the final thickness of the paddle was controlled by both the initial RIE etch (Figure 2b) and the KOH etch time. After etching, the protecting oxide layer was removed with buffered oxide etch (BOE, Transene, a mixture of NH_4F and HF) at room temperature (Figure 3f) to produce a H-terminated surface.

The front and back faces of the micromachined resonators had surfaces of near-atomic smoothness. The morphology of the front face was defined by the BOE etch of the well-annealed oxide coating. This process has been studied in detail previously.[20] The morphology of the paddle backsides, which was determined entirely by the KOH etch, was studied with atomic force microscopy. A typical morphology is shown in Figure 4. As expected, the KOH etch produced Si(111) surfaces of near-atomic flatness.

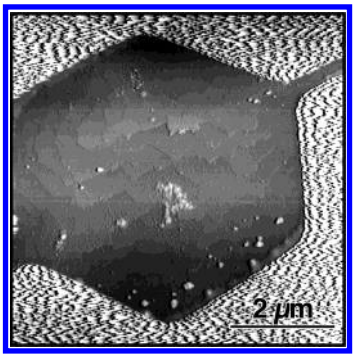

Figure 4. AFM micrograph of the backside of a paddle oscillator showing the very smooth morphology produced by KOH etching. The background "noise" is an artifact of the double-stick tape used to secure the sample, and the white "bumps" are contaminants introduced during mounting.

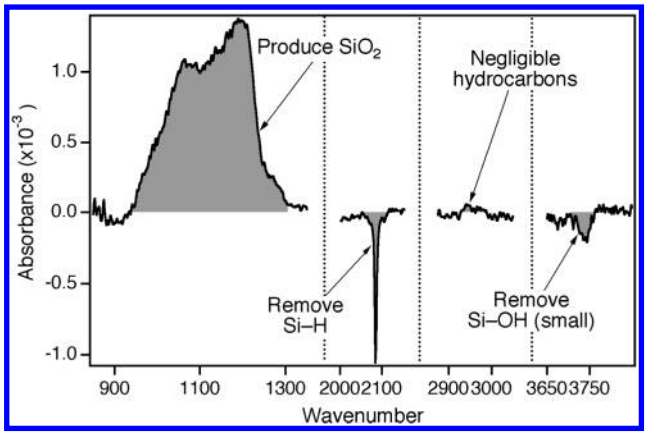

Figure 5. Infrared difference spectrum comparing the oxidized and H-terminated surfaces. Positive peaks indicate species produced during O_3 oxidation, whereas negative peaks indicate species removed during oxidation.

Previous researchers have compared the mechanical properties of oxidized and H-terminated cantilevers;[9,10] however, those experiments used a H atom source to etch away the initial oxide. This process removed a considerable amount of silicon from the cantilevers and produced surfaces with micron-scale roughness.[21] Because of this mass loss, the mechanical properties of oxidized and H-terminated cantilevers could not be compared directly. As a result, surface chemical effects could not be distinguished from stress effects, and the observed changes in dissipation were attributed to stress effects.

The chemical state of our paddles was changed using well-known reactions and was monitored using infrared absorption spectroscopy in transmission mode. Because of the small size of a test chip, infrared spectra were usually obtained from a somewhat larger sample of Si(111) that underwent identical processing. Surfaces terminated with a single monolayer of H atoms were prepared by etching well-cleaned surfaces in room-temperature BOE. The infrared spectrum of wafers prepared in this manner showed a single sharp vibrational resonance at 2083.6 cm^{-1}, which is characteristic of the Si−H stretch vibration on flat (111) terraces.[22] No evidence of surface roughness, oxidation or hydrocarbon contamination was observed. Surfaces terminated with 13 Å of silicon oxide (vide infra) were prepared by exposing the H-terminated surface to UV-generated O_3(g) for 20 min. (During O_3 exposure, the surface was not in line-of-sight of the UV light source.) The chemical state of the oxidized surfaces was verified using infrared absorption spectroscopy. An infrared difference spectrum of the H-terminated and oxidized surfaces is shown in Figure 5. The broad positive band near 1100 cm^{-1} indicates the production of SiO_2 during oxidation, whereas the negative band at 2083.6 cm^{-1} confirms the removal of hydrogen. A small loss of surface silanol groups is also seen. This oxidation process produced no significant hydrocarbon contamination, as verified by the absence of significant absorption in the C−H stretch region near 3000 cm^{-1}.

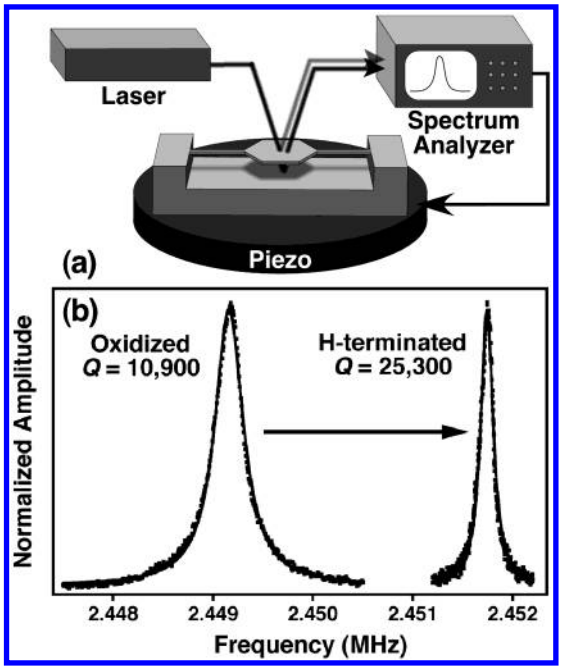

Figure 6. (a) Schematic of interferometric detection apparatus used to characterize resonators. The sample and piezo mounted in high vacuum (10^{-8} Torr). (b) Typical response functions of a single resonator terminated first by a monolayer of H atoms and then by 13 Å of silicon oxide. The solid lines represent best fit Lorentzians.

The resonators' mechanical properties were measured in high vacuum (10^{-8} Torr) by driving the resonators at a variable frequency with a piezoelectric ceramic while monitoring the amplitude of the resonator's motion with a laser interferometer as sketched in Figure 6a. Figure 6b shows typical response curves for the torsional mode of a single oscillator terminated by first a monolayer of hydrogen atoms and then by an ultrathin oxide layer. The solid lines in Figure 6b represent the best fit Lorentzians. Both surface terminations result in sharp vibrational resonances; however, the oxide-terminated resonator has a response that is noticeably broader than that of the H-terminated resonator, indicating that the oxide-terminated resonator has considerably lower Q. The resonator's quality factor can be measured from the response function using the relation

$$Q \equiv \frac{2\pi E}{\Delta E} = \sqrt{1+\sqrt{2}}\frac{f}{\Delta f} \qquad (1)$$

where E is the stored mechanical energy, ΔE is the energy loss per cycle of oscillation, f is the oscillator's resonant frequency, and Δf is the full width at half-maximum of the (Lorentzian) resonant response. For the specific case shown in Figure 6b, oxidation induces a 130% increase in the rate of mechanical energy dissipation and a 0.11% decrease in the resonant frequency. This trend of increasing mechanical energy dissipation and decreasing resonant frequency with oxidation is quite general and observed in all cases.

III. Results

Clearly, resonators with an oxide coating have much lower quality factors than those terminated by a monolayer of H atoms,

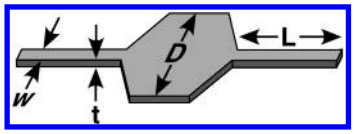

Figure 7. Definition of paddle geometry.

which implies that considerable improvements to current designs might be realized by the development of low-loss surface coatings. But are the oxidation-induced mechanical losses due to an intrinsic increase in surface dissipation? Or are they simply due to chemically induced changes in the stress or tension of the resonators, as has been previously suggested?[9,10]

In the following, we present a series of experiments that demonstrate the following. First, the resonant frequencies of the oscillators are consistent with the well-known bulk properties of silicon; there is no evidence of size dependent changes in the Young's or shear moduli. Second, the resonant frequency shifts induced by oxidation are completely consistent with the addition of a 13 Å layer of silicon oxide; oxidation-induced surface stresses, if any, have a negligible effect on the properties of the resonator. Finally, the size-dependent changes in quality factor are consistent with a surface loss mechanism that occurs over the entire surface area of the resonators (i.e., paddle and wires). Surface-induced losses in only the highly stressed areas of the devices *cannot* account for the observed results.

A. Analysis of Resonant Frequencies. Using a combination of analytic expressions, finite element modeling, and direct measurement, we first confirmed that the static elastic properties of the oscillators (i.e., the elastic moduli) are unaffected by their small size. Two modes of oscillation are observed for each resonator: a translational mode, corresponding to motion of the paddle normal to the hexagonal face, and a torsional mode, corresponding to rotation of the paddle about the wire axis. The frequencies of these modes, which range from 2.2 to 23 MHz, were calculated from the measured dimensions of each oscillator using finite element methods and tabulated mechanical properties of crystalline silicon.

The torsional and translational frequencies of the suspended paddle oscillators were calculated in two steps. First, an analytic expression was derived for the vibration of a rigid hexagonal plate suspended by two flexible beams. This expression captures most of the relevant scaling behavior; however, the neglect of flexure in the plate leads to a systematic overestimate of the resonant frequency. To correct for this, the resonant frequencies of representative paddle geometries were calculated using finite element methods. These calculations included the crystallographic orientation of the paddles and the tensor properties of the elastic response of silicon. By comparing the analytic predictions to the calculated frequencies, a correction constant for both the torsional and translational modes was determined.

The derivation of the analytic expression closely followed the method outlined by Evoy et al.[22] and is described briefly in the following. The translational frequency of a mass M supported by two identical, isotropic rectangular beams of length L, thickness t, width w, and Young's modulus E is given by

$$f_{\text{trans}}^{\text{rigid}} = \frac{1}{2\pi}\sqrt{\frac{k}{M}} = \frac{1}{2\pi}\sqrt{\frac{2Ewt^3}{ML^3}} \tag{2}$$

where k is the spring constant of the beam. Assuming a hexagonal mass with a width across the flats of D, a thickness t and a density ρ, this expression can be further reduced to

$$f_{\text{trans}}^{\text{rigid}} = 0.242\frac{t}{D}\sqrt{\frac{Ew}{\rho L^3}} \tag{3}$$

This geometry is illustrated in Figure 7. The torsional frequency of the same structure is given by

$$f_{\text{tors}}^{\text{rigid}} = \frac{1}{2\pi}\sqrt{\frac{\kappa}{I}} \tag{4}$$

where κ is the torsional stiffness of the supporting beams, and I is the moment of inertia of the hexagonal load. The torsional stiffness of a rectangular beam is given by

$$\kappa = 2\beta G\frac{wt^3}{L} \tag{5}$$

where G is the shear modulus and β is a tabulated constant[24] that is a function of both w and t. Again assuming a hexagonal loading mass, the torsional frequency reduces to

$$f_{\text{tors}}^{\text{rigid}} = 1.03\frac{t}{D^2}\sqrt{\frac{\beta Gw}{\rho L}} \tag{6}$$

To correct these analytic frequencies for flexure in the hexagonal plate, we assume that over the limited range of geometries studied here, the experimental frequencies, f^{exp}, are given by

$$f^{\text{exp}} = cf^{\text{rigid}} \tag{7}$$

where c is a mode dependent constant. Comparing finite element models of a number of our experimental geometries to the predictions of the analytic expressions yielded $c_{\text{trans}}^{\text{calc}} = 0.794$ and $c_{\text{tors}}^{\text{calc}} = 0.926$.

Experimentally, the thickness of the paddles was varied by KOH etching of the paddle backside as described in the Experimental Section. The thickness of the paddle was assumed to vary as

$$t = t_o - rT \tag{8}$$

where t_0 is the initial thickness of the paddle, r is the etch rate of the Si(111) backside (at 70 °C in 50% w/v KOH), and T is the total etch time.

Figure 8 shows the experimentally measured frequencies of our four paddle sizes as a function of KOH etch time. The solid lines represent the best global fit to three parameters: c_{trans}, c_{tors}, and r. The thickness t derived from this fit and eq 8 was in good agreement with direct measurements of the actual thickness taken with a scanning electron microscope. From this fit, we also find that $c_{\text{trans}}^{\text{exp}} = (0.80 \pm 0.36)c_{\text{trans}}^{\text{calc}}$ and $c_{\text{tors}}^{\text{exp}} = (0.46 \pm 0.16)c_{\text{tors}}^{\text{calc}}$. The etch rate of the paddle backside is measured to be 16.6 ± 5.2 nm/min.

The measured translational frequencies were consistent with the calculated frequencies within the error bars of the fit, whereas the measured torsional frequencies were approximately 50% of those calculated. The discrepancy between the calculated and experimental torsional frequencies is likely due to uncertainties in the cross-sectional geometry of the supporting beam. For example, partial faceting of the wire during processing would not be surprising, as the fabrication process involves high-temperature oxidation. Cross-sectional changes would be expected to change the value of β in eq 6.

In summary, the approximate analytic expressions derived above are in good agreement with experiment. Importantly, there

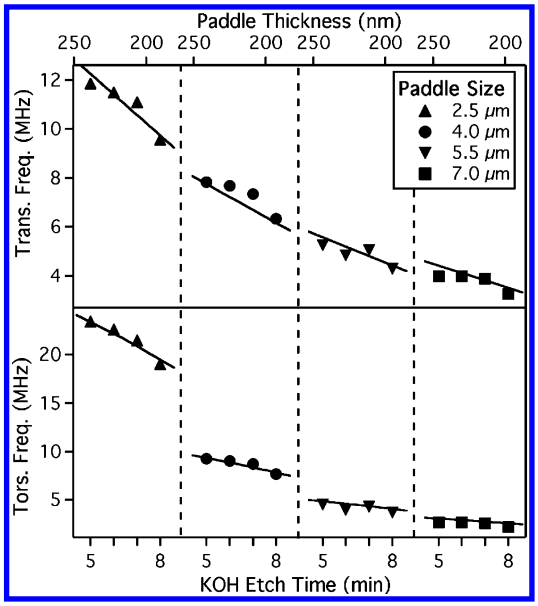

Figure 8. Measured (points) and best global fit (lines) translational and torsional resonant frequencies.

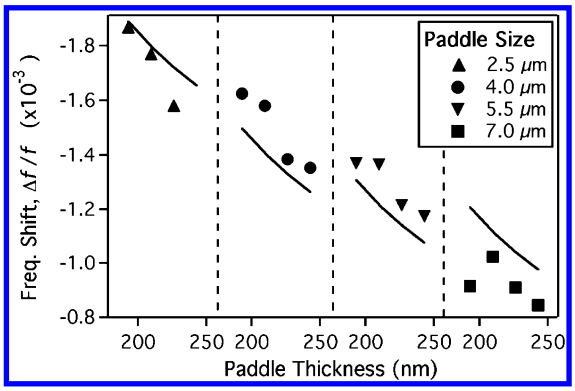

Figure 9. Measured oxidation-induced frequency shifts (points) and best global fit (lines) to eq 14. The single-parameter best fit represents the addition of a 13.0 ± 0.3 Å thick layer of unstressed SiO_2.

is no evidence of size dependent changes in either Young's modulus or in the shear modulus, nor is there any evidence of damage to the bulk silicon lattice. There is no evidence of the anomalous softening which has been reported in previous studies;[23] the resonant frequencies are consistent with the known materials properties of bulk silicon. This finding is in good agreement with previous calculations which predict size-dependent changes in elastic constants only at much smaller dimensions.[25]

The torsional mode was used for the following studies, as this mode is relatively insensitive to bulk thermoelastic losses,[26] mechanical nonlinearities,[23] and changes in drive amplitude. As we will show in the following, uncertainties in the geometry dependent constant β have no effect on the following analysis.

B. Analysis of Frequency Shifts. Since extremely small shifts in resonant frequency are readily detected, the resonant frequency is a sensitive probe of chemical effects. The oxidation-induced frequency shift is defined to be

$$\frac{\Delta f}{f} \equiv \frac{f^{\mathrm{H}} - f^{\mathrm{ox}}}{f^{\mathrm{H}}} \tag{9}$$

where the superscripts H and ox denote H-terminated and oxidized resonators, respectively. As shown in Figure 9, the frequency shift, although extremely small (~0.13%), scales systematically with both paddle size and thickness. In the following, we show that the observed frequency shifts are consistent with the growth of an ultrathin unstressed oxide film. Stress- or tension-induced shifts, if any, are too small to be observable.

In the absence of chemically induced changes in resonator stress or tension, two effects contribute to oxidation-induced changes in torsional frequency. First, the growth of an oxide layer of thickness t_{ox} slightly increases the mass of the resonator and thus lowers the resonant frequency. Second, oxidation consumes a surface layer of thickness t_{Si} of the silicon wire, which lowers the resonant frequency, while producing a somewhat thicker layer of oxide, which raises the resonant frequency. Previous studies of silicon oxidation have shown that $t_{ox} = 2.27 t_{Si}$.[26]

When an infinitesimal dimensional change is made to a hexagonal paddle oscillator, eq 4 predicts that the change in the resonant frequency will be

$$\frac{\partial f}{f} = \frac{1}{2}\frac{\partial \kappa}{\kappa} - \frac{1}{2}\frac{\partial I}{I} \tag{10}$$

In the case of an oxidation-induced change, the moment of inertia changes due to simple mass loading. If a surface layer of thickness ∂t_{Si} and density ρ_{Si} is removed from all surfaces and a surface layer of thickness ∂t_{ox} and density ρ_{ox} is then applied to the paddle, simple geometry predicts that

$$\frac{\partial I}{I} = 2\left(\frac{4}{D} + \frac{1}{t}\right)\left(\frac{\rho_{ox}}{\rho_{Si}} + \frac{\partial t_{Si}}{\partial t_{ox}}\right)\partial t_{ox} \tag{11}$$

(Note that ∂t_{Si} is negative, as it denotes a thickness decrease.) A similar approach is used to calculate the fractional change in the torsional stiffness. In the absence of stress in the oxide (or the Si−SiO_2 interface), the change in torsional stiffness is a simple function of the geometry and materials properties of silicon and silicon oxide. Starting from eq 5, it follows that

$$\frac{\partial \kappa}{\kappa} = \left(\frac{3}{t}\partial t + \frac{1}{w}\partial w\right) \tag{12}$$

During oxidation, both the wire thickness t and the wire width w are first decreased by an amount $2\partial t_{Si}$ and then increased by an amount $2\partial t_{ox}$, which implies that

$$\frac{\partial \kappa}{\kappa} = 2\left(\frac{3}{t} + \frac{1}{w}\right)\left(\partial t_{Si} + \frac{G_{ox}}{G_{Si}}\partial t_{ox}\right) \tag{13}$$

where G is the shear modulus. For the case considered here, the fractional frequency change is very small (~0.13%), and the differential quantities can be converted to differences. Combining eqs 10, 12, and 13 and making use of the previously mentioned relationship $\partial t_{ox} = -2.27 \partial t_{Si}$,[27] the fractional frequency change upon oxidation is given by

$$\frac{\Delta f}{f} = \left[\left(\frac{3}{t} + \frac{1}{w}\right)\left(\frac{G_{ox}}{G_{Si}} - \frac{1}{2.27}\right) - \left(\frac{4}{D} + \frac{1}{t}\right)\left(\frac{\rho_{ox}}{\rho_{Si}} - \frac{1}{2.27}\right)\right]\Delta t_{ox} \tag{14}$$

Equation 14 is a function of known materials properties, the initial dimensions of the paddle oscillator, and a single experimental variable—the thickness of the oxide layer. Importantly, this function is independent of both the scaling parameter c_{tors} and the geometry dependent constant β, which enter into the expression for the initial frequency.

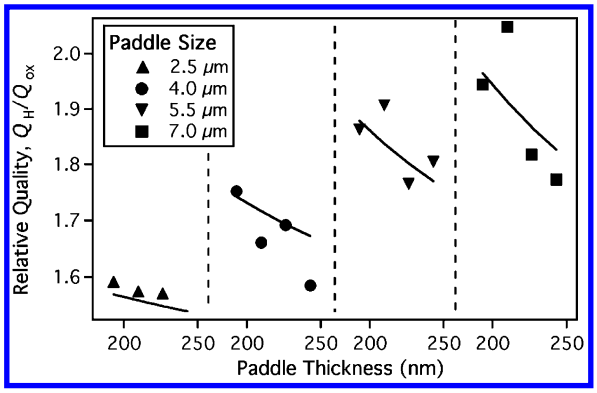

Figure 10. Relative quality of H- and oxide-terminated paddles (points) and best two-parameter global fit (lines) to eq 17.

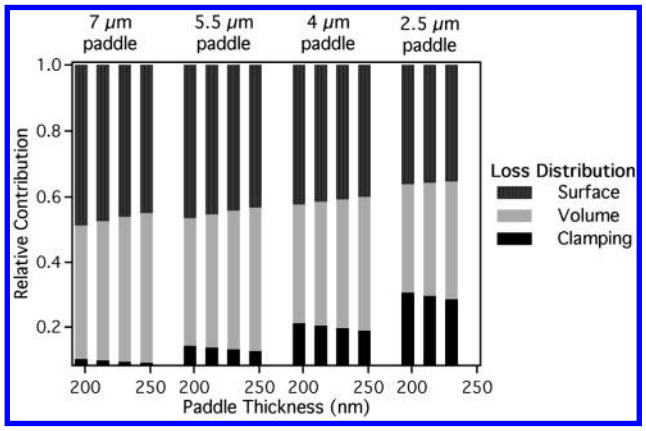

Figure 11. Relative contribution of surface, bulk, and clamping losses to mechanical energy dissipation, as calculated from eq 17 and the best fit in Figure 10.

The solid line in Figure 9 represents the best global fit of the observed frequency shifts to eq 14. The sole fit parameter, the magnitude of ∂t_{ox}, is somewhat dependent on the choice of materials parameters. Especially in the case of silicon oxides, there is some variability in the literature values. In this analysis, the oxide constants were assumed to be $E = 72$ GPa,[28,29] ν (Poisson's ratio) $= 0.20$,[29] and $\rho_{ox} = 2.15$ g cm^{-3}.[30]

The solid line in Figure 9 represents the calculated frequency shift for the replacement of a monolayer of H atoms with a 13.0 ± 0.3 Å thick layer of unstressed silicon oxide. In other words, *less than 2 bilayers of silicon* were oxidized. Depending on experimental conditions, previous researchers have shown that room-temperature oxidation of silicon by O_3(g) produces oxide layers ranging from 7 to 15 Å in thickness,[31,32] which is in good agreement with our measurements. Since the H-terminated Si(111) surface is known to be unstressed, we conclude that stress in the oxide layer is too small to affect the resonant behavior of the device. [Previous measurements have shown that silicon oxidation leads to a small stress that can be either tensile or compressive, depending on the silicon surface.[33]] As a result, the chemically induced changes in dissipation *cannot be attributed* to surface stress, in contrast to previous assertions.[9,10]

This result also highlights the exquisite sensitivity of high-Q resonators to surface modifications—a result that has important implications for sensor technology. For example, the data in Figure 6b suggest that changes in oxide thickness of 0.01 Å could be detected with a signal-to-noise ratio of 3.

C. Analysis of Quality Factors. More insight into mechanical energy dissipation can be obtained from the scaling dependence of the relative quality factors of the hydrogen- and oxide-terminated paddles, Q^H/Q^{ox}, as shown in Figure 10. Interestingly, large paddles are affected more than smaller paddles, which is at first counterintuitive. This effect is not due to size-dependent changes in the magnitude of the stored energy E, as our experiments show that Q is independent of the drive amplitude over a wide range of amplitudes. More surprisingly, the data in Figure 10 show that dissipation is not confined to the highly distorted supporting wires or wire/paddle junctions. Since the nominally high-stress areas, such as the supporting wires and wire/paddle junctions, are conserved across the different paddle geometries (Figure 2), the marked paddle width dependence in Figure 10 must be due to dissipation in regions relatively far from the highly stressed areas.

The scaling of the relative quality provides further proof that oxidation introduces a new surface chemical dissipation mechanism. Using the H-terminated resonator as a fiducial surface, the quality of the resonators can be expressed as

$$Q^H = \frac{2\pi E}{\Delta E} \quad \text{and} \quad Q^{ox} = \frac{2\pi E}{\Delta E + \epsilon} \tag{15}$$

where ϵ represents the oxidation-induced energy loss per cycle of oscillation. Since the measured quality factors are independent of drive amplitude and thus of stored energy, the relative quality is determined by

$$\frac{Q^H}{Q^{ox}} = 1 + \frac{\epsilon}{\Delta E} \tag{16}$$

The term ΔE accounts for all of the energy losses in the H-terminated resonator. This term includes clamping losses, which should be independent of the size of the paddle, and bulk losses [e.g., thermoelastic[26,34] and phonon-mediated[35] losses], which should be proportional to the total volume V of the resonator, including the wire. (We neglect possible chemical losses introduced by the H-terminated surface, due to their relatively small contribution.) Furthermore, since all paddles have the same supporting wires, albeit with a $\pm 10\%$ thickness variation, the clamping losses should be approximately constant for all paddles. The term ϵ accounts for the oxidation-induced losses. If these losses are surface chemical, ϵ should be proportional to the total surface area A of the resonator, including the wires. This simple scaling argument predicts that

$$\frac{Q^H}{Q^{ox}} = 1 + \frac{aA}{V + b} \tag{17}$$

where a and b are size-independent constants. The solid line in Figure 10 represents the best (two-parameter) fit of the data to eq 17, showing that this simple prediction is in good agreement with experiment.

Equation 17 also explains why large paddles are much more sensitive to chemically induced quality changes than small paddles. Since the clamping losses remain roughly constant across the series, increasing the volume of the resonator decreases the relative importance of clamping losses. The fit in Figure 10 implies that over 50% of the losses in the 190 nm thick, 7 μm wide paddle are attributable to surface chemistry. Figure 11 shows the relative contributions of surface, bulk and clamping losses, which are calculated from eq 17, in these devices.

IV. Discussion

The observed surface chemical dependence of mechanical energy dissipation has important implications for future sensor

development. Compared to many nanomechanical structures, the devices studied here have a relatively small surface-area-to-volume ratio and thus relatively low surface chemistry-induced dissipation. For example, the resonator in Figure 1 has approximately 1 surface atom per 600 bulk atoms, whereas high-frequency (380 MHz) nanomechanical silicon wire resonators have approximately 1 surface atom per 50 bulk atoms.[7] According to our analysis, surface chemical losses should be an order of magnitude more important in the nanowires. As a result, replacing the standard oxide coating with a monolayer of H atoms should dramatically improve the quality of these devices (assuming that clamping losses do not dominate.)

These results also suggest that even relatively unstressed areas of the surface can contribute considerably to mechanical energy dissipation. This observation may have important implications for the design of high-Q oscillators. Nevertheless, the mechanism for this dissipation remains unclear. Although the body of the oscillator is relatively unstressed, a small amount of flexure is predicted by the finite element models. This flexure may allow coupling to the surface states (electronic or vibrational).

Although the coupling of macroscopic strain fields to atomic-scale features may at first seem counterintuitive, defect-induced mechanical energy dissipation in bulk materials has been understood in a general sense for more than half a century.[13] When a periodic stress is applied to a material in equilibrium, the chemical bonds surrounding a defect will also be stressed, usually anisotropically. If this stress puts the defect in a nonequilibrium configuration, the defect will move to a new equilibrium geometry *with a finite relaxation time* τ^*. If this relaxation time is comparable to the time scale of the periodic stress, relaxation will occur with a significant phase lag to the applied stress. This phase lag leads to mechanical energy dissipation. As first discussed by Zener,[36] losses in an anelastic solid of this type should obey the relationship

$$\frac{1}{Q} = \frac{E_u - E_r}{\bar{E}} \frac{\omega\tau^*}{1 + (\omega\tau^*)^2} \tag{18}$$

where E_u and E_r describe the elastic response (Young's modulus) of the solid to instantaneous and adiabatic perturbations, respectively. $\bar{E}$ is the geometric mean of E_u and E_r, and ω is the radial frequency of oscillation. Defects are not necessary for dissipation, though. A similar effect occurs when vibrational modes (e.g., phonons) interact with stress fields as first described by Akhiezer.[37]

In principle, electronic and vibrational surface states can couple to a macroscopic distortion in an analogous fashion; however, the relevant state (or states) cannot be identified from the data presented here. What is surprising in this study is not the existence of a surface-mediated dissipation channel, but the relative magnitude of the dissipation. In going from a H-terminated surface to an oxide-coated surface, the rate of mechanical energy dissipation, which is inversely proportional to Q, increases by as much as a factor of 2! In effect, the 13 Å thick silica layer dissipates as much energy as ~1100 Å of bulk silicon even though bulk silica is known to be a low-mechanical-loss material.[12] The magnitude of this effect has important implications for the role of surface chemistry in the production of high-performance nanomechanical devices.

Although the H-terminated silicon surface has much lower losses than the oxidized surface, there is currently no reason to believe that the H-terminated surface has the lowest possible dissipation. Also, our measurements cannot distinguish between dissipation induced by majority species [i.e., hydrogen bound to Si(111) terrace sites] and dissipation induced by defects or minority species [e.g., step sites, impurity or contaminant sites]. Further experiments are clearly needed to determine the chemical parameters that minimize surface dissipation. In addition to the fundamental interest raised by these investigations, the H-terminated silicon surface, although relatively unreactive, may not be sufficiently stable for commercial applications. Because of this, the effects of more robust surface terminations, such as alkane-terminated self-assembled monolayers, on mechanical energy dissipation are currently under investigation. The correlation between chemical functionality and mechanical energy dissipation may also shed light on the underlying mechanism of these losses.

V. Conclusions

Mechanical energy dissipation in micromechanical silicon structures is sensitive to the chemical state of the surface. When a single monolayer of hydrogen atoms is replaced by 13 Å of silicon oxide, which corresponds to the oxidation of less than 2 silicon bilayers, mechanical energy dissipation increases significantly. This effect is not attributable to changes in surface stress or tension, as surface oxidation has a negligible effect on the resonant frequency of the devices. The magnitude of this dissipation is linearly dependent on the entire surface area of the device, not just on the surface area of the highly stressed regions. This scaling suggests that careful attention to surface chemistry will be necessary for the production of high-performance nanoscale resonators.

Acknowledgment. We thank Maxim Zalalutdinov, Jeevak Parpia, and Lidija Sekaric for their invaluable advice. This work was supported by the Cornell Center for Materials Research, a Materials Research Science and Engineering Center of the National Science Foundation (DMR-0079992), and performed in part at the Cornell Nanofabrication Facility (ECS-9731293).

References and Notes

(1) Thundat, T.; Wachter, E. A.; Sharp, S. L.; Warmack, R. J. *Appl. Phys. Lett.* **1995**, *66*, 1695.

(2) Nakagawa, Y.; Schäfer, R.; Güntherodt, H.-J. *Appl. Phys. Lett.* **1998**, *73*, 2296.

(3) Stowe, T. D.; Yasumura, K.; Kenny, T. W.; Botkin, D.; Wago, K.; Rugar, D.; *Appl. Phys. Lett.* **1997**, *71*, 288.

(4) Cleland, A. N.; Roukes, M. L. *Nature* **1998**, *392*, 160.

(5) Nguyen, C. T.-C. *Proceedings 1999 IEEE MTT-S Intl. Microwave Symp. RF MEMS Workshop*, Anaheim, CA, 1999; pp 48−77.

(6) Albrecht, T. R.; Grütter, P.; Horne, D.; Rugar, D. *J. Appl. Phys.* **1991**, *69*, 668.

(7) Carr, D. W.; Evoy, S.; Sekaric, L.; Craighead, H. G.; Parpia, J. M. *Appl. Phys. Lett.* **1999**, *75*, 920.

(8) Yasumura, K. Y.; Stowe, T. D.; Chow, E. M.; Pfafman, T.; Kenny, T. W.; Stipe, B. C. *J. Microelectromech. Sys.* **2000**, *9*, 117.

(9) Yang, J.; Ono, T.; Esashi, M. *Appl. Phys. Lett.* **2000**, *77*, 3860.

(10) Yang, J.; Ono, T.; Esashi, M. *J. Vac. Sci. Technol. B* **2001**, *19*, 551.

(11) Mihailovich, R. E.; Parpia, J. M. *Phys. Rev. Lett.* **1992**, *68*, 3052.

(12) Penn, S. D.; Harry, G. M.; Gretarsson, A. M.; Kittelberger, S. E.; Saulson, P. R.; Schiller, J. J.; Smith, J. R.; Swords, S. O. *Rev. Sci. Instrum.* **2001**, *72*, 3670 and references therein.

(13) Calculated from Braginsky, V. B.; Mitranov, V. P.; Panov, V. I. *Systems with Small Dissipation*; University of Chicago Press: Chicago, 1985; Chapter 2.

(14) Higashi, G. S.; Chabal, Y. J.; Trucks, G. W.; Raghavachari, K. *Appl. Phys. Lett.* **1990**, *56*, 656.

(15) Yablonovitch, E.; Allara, D. L.; Chang, C. C.; Gmitter, T.; Bright, T. B. *Phys. Rev. Lett.* **1986**, *57*, 249.

(16) Raghavachari, K.; Jakob, P.; Chabal, Y. J. *Chem. Phys. Lett.* **1993**, *206*, 156.

(17) Ensell, G. *J. Micromech. Microeng.* **1995**, *5*, 1.

(18) Flidr, J.; Huang, Y.-C.; Hines, M. A. *J. Chem. Phys.* **1999**, *111*, 6970.
(19) Wind, R. A.; Jones, H.; Little, M. J.; Hines, M. A. *J. Phys. Chem. B* **2002**, *106*, 1557.
(20) Garcia, S. P.; Bao, H.; Hines, M. A. *Surf. Sci.* **2003**, *541*, 252.
(21) See Figure 3 of ref 10.
(22) Jakob, P.; Chabal, Y. J. *J. Chem. Phys.* **1991**, *95*, 2897.
(23) Evoy, S.; Carr, D. W.; Sekaric, L.; Olkhovets, A.; Parpia, J. M.; Craighead, H. G. *J. Appl. Phys.* **1999**, *86*, 6072.
(24) Ford, H. *Advanced Mechanics of Materials*; Wiley: New York, 1963; p 380.
(25) Broughton, J. Q.; Meli, C. A.; Vashishta, P.; Kalia, R. K. *Phys. Rev. B* **1997**, *56*, 611.
(26) Houston, B. E.; Photiadis, D. M.; Marcus, M. H.; Bucaro, J. A.; Liu, X.; Vignola, J. F. *Physica B* **2002**, *316*−*7*, 408.
(27) Ghandi, S. K. *VLSI Fabrication Principles*; Wiley: New York, 1983; p 377.
(28) Auld, B. A. *Acoustic Field and Waves in Solids*; Wiley: New York, 1973; Vol. 2, p 368.
(29) Carlotti, G.; Douce, L.; Dupeux, M. *J. Vac. Sci. Technol. B* **1989**, *7*, 153.
(30) Ghandi, S. K. *VLSI Fabrication Principles*; Wiley: New York, 1983; p 388.
(31) Lau, W. M.; Huang, L. J.; Chang, W. H.; Vos, M.; Mitchel, I. V. *Appl. Phys. Lett.* **1993**, *63*, 78.
(32) Maeda, T.; Kurokawa, A.; Sakamoto, K.; Ando, A.; Itoh, H.; Ichimura, S. *J. Vac. Sci. Technol. B* **2001**, *19*, 589.
(33) Sander, D.; Ibach, H. *Phys. Rev. B* **1991**, *43*, 4263.
(34) Lifshitz, R.; Roukes, M. L. *Phys. Rev. B* **2000**, *61*, 5600.
(35) Lifshitz, R. *Physica B* **2002**, *316*−*7*, 397.
(36) Zener, C. *Elasticity and Anelasticity of Metals*; University of Chicago Press: Chicago, 1948.
(37) Akhiezer, A. *Zh. Eksp. Teor. Fiz.* **1938**, *8*, 1318.